THE JOURNAL OF PHYSICAL CHEMISTRY A

 VOLUME 107, NUMBER 30, JULY 31, 2003

ARTICLES

Probing the Spectral Diffusion of Vibrational Transitions of OCN^- and SCN^- in Methanol by Three-Pulse Infrared Photon Echo Spectroscopy

Kaoru Ohta,[†] Hiroaki Maekawa,[†] Shinji Saito,[‡] and Keisuke Tominaga*[,†,§]

Graduate School of Science and Technology, Kobe University, Nada-ku, Kobe 657-8501, Japan, Chemistry Department, Faculty of Science, Nagoya University, Furo-cho, Chikusa-ku, Nagoya 464-8602, Japan, and Molecular Photoscience Research Center, Kobe University, and CREST, JST, Japan Science and Technology Corporation, Nada-ku, Kobe 657-8501, Japan

Received: February 12, 2003; In Final Form: May 5, 2003

Three-pulse infrared photon echo spectroscopy has been used to determine the correlation function of the fluctuations of the vibrational frequencies of OCN^- and SCN^- in methanol. The correlation functions of the antisymmetric stretching modes for these two ions are fitted with a double exponential function with time constants of around 100 fs and 4 ps. The amplitude of the fluctuations for SCN^- is found to be greater than that for OCN^-. We discuss the difference of the spectral diffusion processes between OCN^- and SCN^- in methanol.

1. Introduction

Molecular dynamics in liquids are strongly affected by the nature of intermolecular interactions. It is greatly important to obtain the molecular description on relation between the dynamics and interactions in liquids in order to elucidate the solvent dynamical effect on chemical reactions. Fluctuations of the vibrational transition energies, which are characterized by time correlation functions of the frequency fluctuations, are very sensitive to the dynamics of surrounding environments.[1] Therefore, it has been expected to investigate the microscopic view on liquid dynamics by probing the vibrational fluctuations.

In recent years, a great deal of effort has been devoted to investigate solute−solvent interactions and vibrational frequency fluctuations with nonlinear infrared (IR) spectroscopy.[2−10] These techniques give detailed information on the time scale of the vibrational fluctuation and the coupling strength to the solvent. Although spectroscopic line shape measurement is a common technique to study the microscopic aspect in liquids, it does not always give the underlying physical picture of the vibrational dynamics. Recently, two-dimensional (2D) IR spectroscopy, a vibrational analogue of 2D NMR, has been proven to be a powerful technique to study dynamical structures of molecular systems and biopolymers.[4−7]

Three-pulse photon echo measurements are a useful technique to probe energy fluctuations of optical transitions or spectral diffusions. This is because echo signals with three-pulse excitations can yield the dynamics of the inhomogeneous distribution,[11] while the static inhomogeneous distribution of the transition frequency can be obtained by two-pulse photon echo measurements.[2] The three-pulse technique has been applied to electronic transitions[12,13] and, more recently, to vibrational transitions for small molecules in solutions[14] and in protein environments.[15] This nonlinear spectroscopy is especially powerful when the spectral diffusion process is characterized by multiple time scales.

In this work we have studied spectral diffusion or solvation dynamics of the vibrational states for triatomic ions such as OCN^- and SCN^- in methanol. Studies on simple triatomic ions

* Corresponding author. E-mail: tominaga@kobe-u.ac.jp. Phone: +81-78-803-5684. Fax: +81-78-803-5684.
[†] Graduate School of Science and Technology, Kobe University.
[‡] Nagoya University.
[§] Molecular Photoscience Research Center, Kobe University, and CREST, JST, Japan Science and Technology Corporation.

10.1021/jp034362f CCC: $25.00
Published on Web 07/09/2003

TABLE 1: Parameters of the Vibrational Population Relaxation Times, Rotational Diffusion Constants, and Anharmonicities for OCN^- and SCN^- in Methanol

solute	T_1[a] (ps)	rotational diffusion constant[a] (ps^{-1})	anharmonicity[a] (cm^{-1})
OCN^-	2.9	0.025	28
SCN^-	11.0	0.019	23

solute	peak frequency in methanol (cm^{-1})	peak frequency in gas phase[a] (cm^{-1})	line width[a] (cm^{-1})
OCN^-	2161	2124.3	20
SCN^-	2062[b]	2065.9	45

[a] Taken from ref 19. [b] Peak frequency is determined by fitting with a Gaussian function, since the absorption spectrum is slightly asymmetric. The actual peak is shifted slightly to a lower frequency.

provide detailed physical origins on solute−solvent interactions and serve as a benchmark for theoretical modeling. Fundamental parameters are already available on the vibrational states for the ions both in gas phase and in solutions (Table 1).[16−20] Despite their simple structures, the triatomic ions show interesting features regarding vibrational interactions and dynamics.

In the previous pump−probe experiments by Hochstrasser and co-workers, the vibrational population relaxation times were measured for N_3^-, OCN^-, and SCN^- in several solvents.[19,20] They suggested that the longer vibrational relaxation time and shorter reorientation time for SCN^- are due to weak interactions with solvent compared to the cases of N_3^- and OCN^-. Furthermore, the trend in the vibrational relaxations correlates with the shift of the peak frequency between the solvent and the gas phase. On the other hand, the line width of the absorption spectrum of the antisymmetric stretching mode of SCN^- is broader than that of OCN^-, indicating the stronger solute−solvent interactions for SCN^-. There is no explanation for these different trends even though quantitative information on the vibrational dynamics of ions is experimentally available.[19,20] It is necessary to investigate the vibrational dephasing dynamics of ions in order to elucidate the line broadening mechanism of the absorption spectrum. In this study, vibrational frequency correlation functions of the antisymmetric stretching modes for OCN^- and SCN^- are determined by three-pulse IR photon echo experiments. We discuss the difference of the spectral diffusion processes between OCN^- and SCN^- in methanol.

2. Experimental Section

The details of three-pulse IR photon echo measurement will be described elsewhere.[21] Briefly, a laser system was based on a Ti:sapphire regenerative amplifier (Spitfire, Spectra Physics) to provide pulses with a pulse width of about 40 fs and an energy of 1 mJ/pulse at 1 kHz centered at around 800 nm. The output is used to pump an optical parametric amplifier (OPA), and difference frequency generation of the signal and idler from the OPA in $AgGaS_2$ is used to produce tunable IR pulses (140−160 fs pulse width, 120−130 cm^{-1} bandwidth).[22] The resulting IR pulses were tuned to around 2150 and 2054 cm^{-1} for OCN^- and SCN^-, respectively. The IR beam was split into three and was focused at the sample with an off-axis parabolic reflector (focal length = 100 mm) in a boxcar geometry. At a sample position, a pulse energy was ∼2−3 μJ in total. Time delays between two beams are independently controlled with motorized stepper translation stages. The photon echo signal was detected with a liquid N_2 cooled InSb detector in the phase matched direction, $-\mathbf{k_1} + \mathbf{k_2} + \mathbf{k_3}$, where $\mathbf{k_1}$, $\mathbf{k_2}$, and $\mathbf{k_3}$ are the wavevectors of the first, second, and third pulses, respectively. The time delay between the $\mathbf{k_1}$ and $\mathbf{k_2}$ beams is defined as τ, while T is defined as the time delay between the $\mathbf{k_2}$ and $\mathbf{k_3}$ beams for $\tau > 0$ or between the $\mathbf{k_1}$ and $\mathbf{k_3}$ beams for $\tau < 0$.

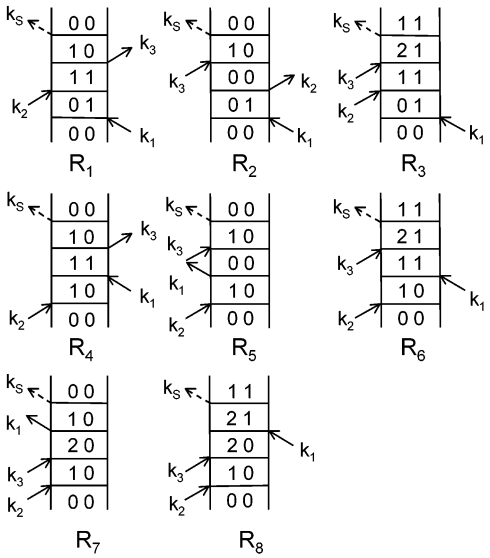

Figure 1. Double-side Feynman diagrams that contribute to the photon echo signals.

KOCN, KSCN, and methanol (spectrograde) were purchased from WAKO Pure Chemical Industries and were used without further purification. The sample was a 45 mM solution for OCN^- and a 160 mM solution for SCN^- in methanol in a CaF_2 cell with an optical path length of 50 μm. All measurements were performed at ambient temperature (295 K).

3. Theory

The experimentally observed photon echo signal is a time-integrated intensity of the third-order polarization which is given by

$$I(\tau,T) \propto \int_0^\infty |P(t;T,\tau)|^2 \, dt \qquad (1)$$

where $P(t;T,\tau)$ is the third-order nonlinear polarization at time t. The third-order polarization is expressed by convolution of the response function with the electric fields of the laser pulses.[23] The detailed description of the response functions was given by Mukamel[23] and others.[14,24] Briefly, the relevant Feynman diagrams for the photon echo signal are shown in Figure 1. The response function is a sum of contributions from all the Feynman paths. The first three diagrams contribute to the photon echo signal when the delay time τ is positive. These are so-called rephasing diagrams which give photon echo signals. For example, in the diagram R_1, the first pulse creates a vibrational coherence between $v = 0$ and $v = 1$ states that is destroyed by the dephasing process. After time τ, the population in the $v = 1$ state is created after the second interaction of the laser pulse. The third pulse transfers the second coherence state which is the conjugate of the first one. So the system propagates toward the initial coherence, giving the echo signals. Among the rest of the diagrams, the diagrams R_4, R_5, and R_6 contribute to the signal when the delay time τ is negative. These are so-called non-rephasing diagrams which give free induction decays because the second coherence state has the same phase factor (not conjugate) as the first one that is also destroyed by the dephasing process. The last two diagrams R_7 and R_8 contribute to the signals only when the delay time T is near zero. The inhomogeneous distribution of the vibrational frequency causes

a greater rephasing contribution than the non-rephasing one, so that the peak of the photon echo signal is located at the positive side of τ when the delay time τ is scanned with a fixed T.[11] As the delay time T increases, molecular dynamics in liquids destroy the inhomogeneity of the distribution of the vibrational frequencies. When there is no inhomogeneity in the system or the inhomogeneity is washed out completely due to the spectral diffusion, rephasing and non-rephasing diagrams contribute equally to the signals, and the photon echo signal becomes symmetric with respect to $\tau = 0$ fs. Therefore, the asymmetry of the photon echo signals is a sensitive probe for the degree of the "transient" inhomogeneity in the distribution of the vibrational frequencies.

The spectral diffusion process is described by the correlation function of the vibrational frequency fluctuation which is given by

$$M(t) = \langle \delta\omega_{01}(t)\, \delta\omega_{01}(0) \rangle \tag{2}$$

where $\delta\omega_{01}(t)$ is the deviation of the vibrational frequency at time t from the average value.[11] Here we assume that the fluctuations of the vibrational energy between $v = 0-1$ and $v = 1-2$ are strongly correlated, that is, that $\delta\omega_{01}(t)$ is equal to $\delta\omega_{12}(t)$. The response function can be calculated from the line shape function $g(t)$,

$$g(t) = \int_0^t \mathrm{d}t_1 \int_0^{t_1} \mathrm{d}t_2 \, \langle \delta\omega_{01}(t_2)\, \delta\omega_{01}(0) \rangle \tag{3}$$

The relation between the response function and the line shape function has been described in other papers.[14,24] In the following simulation, we take into account the effect of the finite pulse width, the lifetime contribution, and the rotational relaxation process following Hamm et al.[14,24] A contribution of the vibrational population relaxation is included phenomenologically as an exponentially decaying factor. When the system is in $v = 0-1$ coherence, the decay rate is $^1/_2T_1$, and when the system is in $v = 1-2$ coherence, there is an additional contribution of $1/T_1$. During the population period, the decay rate is $1/T_1$. T_1 is the vibtational population relaxation time from the $v = 1$ to the $v = 0$ state. Here we assume that the vibrational relaxation from the $v = 2$ to the $v = 1$ state is twice as fast as that from the $v = 1$ to the $v = 0$ state. This assumption is based on the harmonic approximation for the transition dipole moment, that is, $2\mu_{10}^2 = \mu_{21}^2$. The transition rate is given by the Fermi's golden rule and is linear in the vibrational quantum number for the harmonic oscillator.[25] Regarding the rotational relaxation, we assume the system can be described by a spherical rotor. During $v = 0-1$ and $v = 1-2$ coherence, the rotational dephasing rate is $2D$, and during the population period, the rate is $6D$, where D is the rotational diffusion constant.[26] A contribution of each diagram R_1-R_8 depends on the time ordering of the three pulses, and all of the diagrams are included in the calculation, as shown below.

4. Results

Figure 2a shows the three-pulse photon echo signals of OCN^- in methanol as functions of the delay times τ and T. At $T = 0$ fs the peak of the photon echo signal is located at around 300−350 fs. The temporal profile of the photon echo signal is highly asymmetric with respect to τ, indicating the presence of the inhomogeneous distribution of the vibrational frequency. The peak of the signal shifts toward zero as T increases. To characterize the degree of asymmetry of the photon echo signals with respect to $\tau = 0$ fs, the first moments of the echo signals

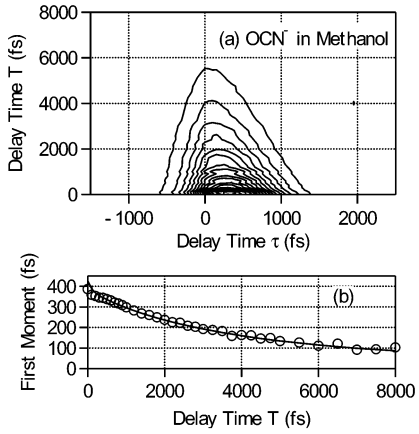

Figure 2. (a) Three-pulse photon echo signals plotted against the delay times τ and T for OCN^- in methanol. (b) First moment of the photon echo signals from the experimental data (open circles) and from the simulation (solid line).

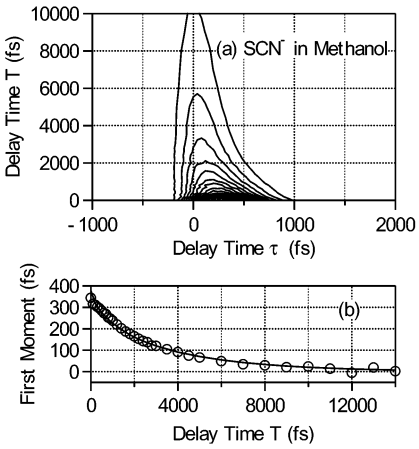

Figure 3. (a) Three-pulse photon echo signals plotted against the delay times τ and T for SCN^- in methanol. (b) First moment of the photon echo signals from the experimental data (open circles) and from the simulation (solid line).

are calculated as a function of T, as shown in Figure 2b. The first moment is defined as follows,

$$FM(T) = \frac{\int_{-\infty}^{\infty} \tau I(\tau,T)\, \mathrm{d}\tau}{\int_{-\infty}^{\infty} I(\tau,T)\, \mathrm{d}\tau} \tag{4}$$

where $I(\tau,T)$ is the experimental photon echo signal at the delay times τ and T. The first moment is around 400 fs at $T = 0$ fs and decays to 100 fs on a time scale of 4 ps. The total intensity of the photon echo signals decreases on a few picosecond time scale, since the vibrational relaxation time of the antisymmetric stretching mode of OCN^- in methanol is 3 ps.[19,20] Therefore, it is difficult to measure the signal at delay time T longer than 8 ps.

Figure 3 shows the photon echo signals of SCN^- in methanol as functions of the delay times τ and T together with the time dependence of the first moment. The temporal width of the photon echo signal for SCN^- is narrower than that for OCN^-. Decay of the echo signal is related to the vibrational dephasing time. In a motionally narrowing limit, the vibrational dephasing time is inversely proportional to the square of the coupling strength to solvent. Therefore, a faster decay of the photon echo signal for SCN^- reflects a stronger system−bath interaction for SCN^- compared to OCN^- and is consistent with the difference

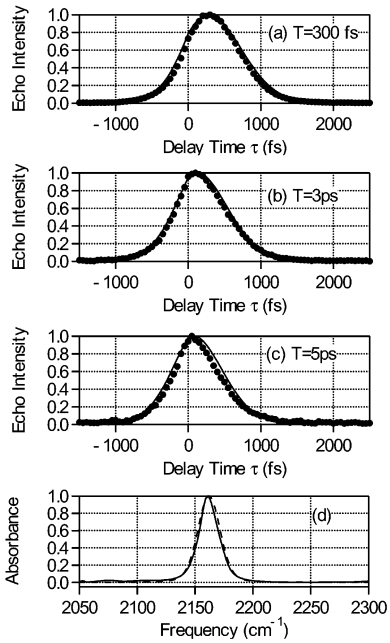

Figure 4. Three-pulse photon echo signals of OCN^- in methanol at three different delay times *T*: (a) 300 fs; (b) 3 ps; (c) 5 ps. The filled circles represent the experimental data, and the solid line represents the simulated data. (d) Experimental linear absorption spectrum of OCN^- in methanol (solid line). The dashed line is calculated from the simulation using the parameters shown in Tables 1 and 2.

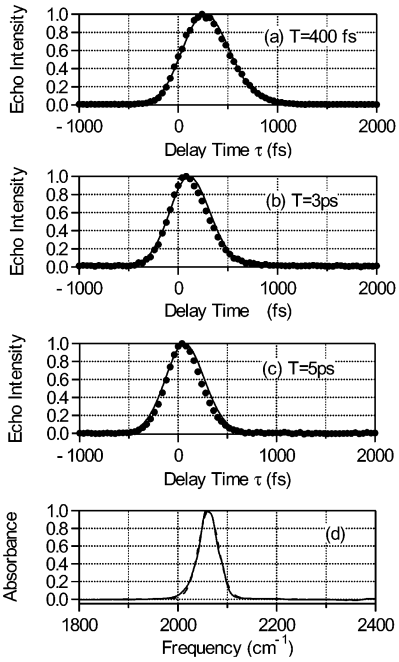

Figure 5. Three-pulse photon echo signals of SCN^- in methanol at three different delay times *T*: (a) 400 fs; (b) 3 ps; (c) 5 ps. The filled circles represent the experimental data, and the solid line represents the simulated data. (d) Experimental linear absorption spectrum of SCN^- in methanol (solid line). The dashed line is calculated from the simulation using the parameters shown in Tables 1 and 2.

TABLE 2: Parameters of the Correlation Function for OCN^- and SCN^- in Methanol

solute	Δ_1 (ps^{-1})	τ_1 (ps)	Δ_2 (ps^{-1})	τ_2 (ps)	Δ_0 (ps^{-1})
OCN^-	1.3	0.12	1.6	4.5	0.55
SCN^-	2.6	0.09	3.6	4.1	0.1

of the width of the absorption spectra observed between OCN^- and SCN^-.[19,20] The first moment of the photon echo signal at $T = 0$ fs is similar to that for OCN^-, but it decays to zero, indicating that there is very small static inhomogeneity at a longer delay time *T*. For SCN^- in methanol, the vibrational population relaxation occurs on a 11 ps time scale,[19,20] so we can measure the photon echo signals easily at the delay time *T* longer than 10 ps.

To simulate the photon echo signals, the correlation function of the vibrational frequency fluctuation is expressed by a sum of two exponentials with a constant term,

$$M(t) = \sum_{i=1}^{2} \Delta_i^2 \exp(-t/\tau_i) + \Delta_0^2 \qquad (5)$$

Here Δ_i and τ_i correspond to the coupling strength to solvent and the time scale of the frequency fluctuation, respectively. We calculated the temporal profile of the photon echo signal at each delay time *T* according to eq 1, taking into account the pulse width and the time ordering of the laser pulses, and then the first moment of the photon echo signal was calculated on the basis of eq 4. A comparison of calculated signals with the experimental results for OCN^- in methanol is displayed in Figure 4a−c. The parameters used in the simulation are shown in Table 2. $M(T)$ has two decaying time constants of 120 fs and 4.5 ps. We include a constant term in $M(T)$, Δ_0, which corresponds to a component longer than the time scale of our measurement (∼8 ps). Calculated and observed absorption spectra are shown in Figure 4d. The absorption spectrum is calculated from the following equation.

$$I(\omega) = 2\mathrm{Re}\int_0^\infty \exp[-i(\omega - \omega_{01})t] \exp[-g(t) - t/2T_1 - 2Dt]\, dt \qquad (6)$$

The overall fit is good; however, there are some differences between the experimental and simulated results. In particular, the deviation of the first moment from the experimental data is seen at the delay time *T* shorter than 400 fs, and the temporal width of the photon echo signals is slightly overestimated at a longer *T*. The calculated absorption spectrum overestimates the width of the experimental absorption spectrum, too. One of the reasons may be a contribution of a small fifth-order polarization to the photon echo signals. We have observed a small fifth-order contribution to the photon signals in the frequency-resolved photon echo measurements.[27] The fifth-order contribution gives a shoulder in the spectrum at the lower frequency side, which is due to $v = 2-3$ coherence. This observation is similar to that reported by Hochstrasser and co-workers.[28,29]

The simulated result for SCN^- in methanol is shown in Figure 5 along with the experimental absorption spectrum and photon echo signals. The simulated result for SCN^- shows very small static inhomogeneity after 14 ps. It is notable that the time constants of the frequency fluctuations for two components are quite similar for SCN^- and OCN^-, while the amplitudes of the fluctuations for SCN^- are about twice as large as those for OCN^-. For both molecules, the contribution of the population relaxation of the $v = 1$ state and the rotational relaxation to the vibrational dephasing process is found to be minor in the photon echo signals. The accuracy of the parameters for the first component, τ_1 and Δ_1, is relatively large, probably about ±50%. This is because this component falls into the fast modulation limit and only the values of $\Delta_1^2\tau_1$ are important to determine the vibrational dephasing.

TABLE 3: Bond Lengths, Magnitudes of Dipole Moments, and Atomic Charges of OCN^- and SCN^-

	bond length		
solute	R_{SC} or R_{OC} (Å)	R_{CN} (Å)	μ (D)
OCN^-	1.2320	1.2017	1.4805
SCN^-	1.6609	1.1908	1.5823

	atomic charge		
solute	S or O	C	N
OCN^-	−0.606	0.166	−0.560
SCN^-	−0.629	−0.047	−0.324

TABLE 4: Coefficients of the Normal Coordinate of the Antisymmetric Stretching Mode for OCN^- and SCN^-

	coefficient of the normal coordinate		
solute	S or O	C	N
OCN^-	−0.26	0.86	−0.44
SCN^-	−0.05	0.81	−0.59

We have performed ab initio calculation on OCN^- and SCN^- in a vacuum by the Gaussian program to investigate molecular structures and the charge distribution of the ions.[30] Several different basis sets are used such as 6-311G,[31] cc-pVDZ,[32,33] or cc-pVTZ.[32,33] The results on the structure, dipole moment, and charge distribution are summarized in Table 3. The geometries of ions are optimized by the MP2 calculation with the cc-pVTZ basis set. The charges on atoms are calculated with Mulliken population analysis.[34] The origin of the molecular coordinate to estimate the dipole moment is defined to be a center of mass of the charge distribution of nuclei. The charge distributions for OCN^- and SCN^- are slightly different. In OCN^- the charge is equally located at the N and O ends. In SCN^-, the magnitude of the atomic charge at the S end is larger than that at the N end. The dipole moments are almost the same for both ions. This tendency is independent of the basis set though the absolute value of the dipole moment is somewhat dependent on it. The coefficients of the normal coordinate of the antisymmetric stretching mode are shown in Table 4, which are obtained from the MP2 calculation with the cc-pVTZ basis set. As pointed out previously,[19] the vibrational motion of the antisymmetric stretching is localized in the CN part for SCN^- while it is delocalized in the whole molecule for OCN^-.

5. Discussion

We have obtained the correlation functions of the frequency fluctuations for the antisymmetric stretching modes of OCN^- and SCN^- in methanol by means of three-pulse photon echo spectroscopy. The obtained parameters of the correlation functions are summarized in Table 2, and one of the major conclusions of this work is that the decays of the correlation functions of both ions have similar time scales despite a large difference in the coupling strength. This indicates that the solvation dynamics of the vibrational modes are determined by similar underlying dynamics for both cases; the time dependence of the fluctuation is independent of the strength of the interaction. We will discuss the natures of the interactions and dynamics, and relations of the spectral diffusion with other vibrational quantities.

In the previous three-pulse IR photon echo studies of N_3^- in D_2O by Hamm et al., the correlation function decays with time constants of 80 fs and 1.3 ps.[14] On the basis of the results of the molecular dynamics simulation done by Ferrario et al., the slowly decaying component of the correlation function corresponds to the fluctuations of the vibrational force resulted from making and breaking of the hydrogen bonds.[35] The fast decaying component is assigned to the inertial part of the water solvation on the basis of the observation of a similar component in the dynamic fluorescence Stokes shift measurement for the electronic transition.[14] Preliminary experiments for probing the vibrational frequency fluctuations for the CN stretching mode of $Fe(CN)_6^{4-}$ and the antisymmetric stretching mode of SCN^- in D_2O suggest that the correlation function decays on similar time scales to that for N_3^- in D_2O.[14,21] The time constants of the slowly decaying component for OCN^- and SCN^- in methanol are clearly different from those of the ions in D_2O while all the systems studied have fast decaying components with a time constant of about 100 fs. On the other hand, the amplitude of the vibrational energy fluctuation for the slowly decaying component is larger than that in D_2O. The results of molecular dynamics simulations on CN^- in water and methanol suggested that the time scale of the making and breaking of the hydrogen bonds in methanol is about three times (for CN^-) slower than that in water.[36] Furthermore, molecular dynamics calculations for N_3^- in methanol showed that the "hydrogen bond" lifetime in methanol is 2.1 ps.[35] This suggests that the slow components with time constants of about 4 ps result from the hydrogen bond breaking and making dynamics. The fast components of about 100 fs are probably due to the inertial component of the methanol solvation, similarly to the D_2O solution cases. All the results indicate that the dynamics of the vibrational frequency fluctuations of the ions are mainly determined by solvent nature and not by the solute character, while the coupling strength depends on both the solvent and solute.

Interpretation of the difference of the spectral diffusion process of OCN^- and SCN^- in methanol is not straightforward. First we consider the relation between the vibrational population relaxation and the vibrational dephasing process for OCN^- and SCN^- in methanol. There are two pathways for the vibrational relaxation process, either the direct relaxation to the ground state or intramolecular vibrational energy redistribution (IVR) to the other modes. Vibrational population relaxation can be described by the Laudau−Teller formula.[37,38] According to this formula, the rate of the direct vibrational relaxation, k, for a model diatomic solute is given by

$$k = \frac{1}{mk_BT}\int_0^\infty \mathrm{d}t\, \cos(\omega t)\langle F(t)\, F(0)\rangle \qquad (7)$$

where m is the reduced mass of the vibrational mode in question and k_BT is the thermal energy of the system. $F(t)$ is the time-dependent force exerted by the solvent molecules on the solute vibrational mode, which is given by the first-order derivative of the solute−solvent interaction with respect to the vibrational coordinate. On the other hand, the correlation function of the vibrational frequency within the framework of the perturbation theory is given by[39]

$$\langle \delta\omega_{01}(t)\, \delta\omega_{01}(0)\rangle = \left(\frac{f}{2m^2\omega^3}\right)^2 \langle F(t)\, F(0)\rangle + \left(\frac{1}{m\omega}\right)^2 \langle G(t)\, G(0)\rangle \qquad (8)$$

where f is the cubic anharmonicity of the vibrational Hamiltonian and G is the second derivative term of the solute−solvent interaction. If the oscillator is harmonic, only the second term of eq 8 contributes to the correlation function.

In the previous pump−probe experiments by Hochstrasser and co-workers, longer vibrational relaxation time for SCN^- is observed, suggesting weak solvent interactions compared to the case of OCN^-.[19,20] Furthermore, a longer vibrational relaxation time of N_3^- in the aprotic solvent HMPA (14.8 ps) is observed compared to that in methanol (2.4 ps), demonstrating the importance of hydrogen bond interactions in the relaxation pathway.[19] Therefore, a stronger solute−solvent interaction for OCN^- gives the greater coupling strength in the vibrational frequency correlation function and thus a larger amplitude of the fluctuations in the vibrational transition frequency if the direct relaxation to the ground state dominates in the overall vibrational population relaxation process. If both the vibrational population relaxation (eq 7) and the frequency fluctuation (eq 8) are determined by only the correlation function of $F(t)$, we could evaluate the vibrational population relaxation rates for OCN^- and SCN^- on the basis of the parameters obtained from the photon echo measurements. But there are a couple of problems on this issue. First, the constant offset in $M(T)$ is not well defined, particularly for OCN^-, which causes difficulty to perform the integral in eq 7. Second, the parameters in $M(T)$ do not have detailed information to describe the short-time dynamics, which leads to uncertainty of the power spectrum of the correlation function in the high frequency side. Therefore, the following discussion is limited only to a qualitative level.

Theoretical studies of N_3^- in water by Morita and Kato showed that the direct relaxation to the ground state and the IVR to the symmetric stretching mode equally contribute to the overall vibrational population relaxation, and the charge fluctuation effect of the ion greatly enhances the relaxation rate of both the processes.[40] The contribution of the IVR process to the overall rate could be different between OCN^- and SCN^-, giving different vibrational population relaxation times. For the IVR process, the excitation energy flows to the symmetric stretching and bending modes. The frequencies of the symmetric stretching and bending modes for OCN^- are higher than those for SCN^-.[16,17] Less energy gap between these modes could give a more efficient IVR process for OCN^-. For the vibrational population relaxation, only the first-order derivative of the solute−solvent interaction is usually considered, as shown in eq 7, and the higher-order derivative terms such as the G term are neglected. However, the relative importance of the first term to the second term of eq 8 for the correlation function of the vibrational frequency is not clear for the present system. For the molecular dynamics simulation of CN^- in water, it was found that the vibrational dephasing of the CN stretching mode is mainly due to the first term of eq 8.[41] Further studies are necessary to address this point for OCN^- and SCN^-. Regarding the different behaviors for the vibrational population relaxation and the spectral diffusion process, we consider that the IVR process may play an important role in the population relaxation and the G term in eq 8 could be a major factor in the vibrational frequency correlation functions. The force acting on a vibrational coordinate depends on the charge distribution and the form of the normal coordinates of the ions, causing different contributions to the vibrational population relaxation and vibrational dephasing process.

Regarding the gas-to-solution solvent shifts, the frequencies of the antisymmetric stretching modes for OCN^- and SCN^- in the gas phase are 2124.3 and 2065.9 cm^{-1}, respectively. The peak frequency is higher by about 37 cm^{-1} for OCN^- in methanol than that in the gas phase, while there is a small shift in SCN^-.[19,20] These trends correlate with the vibrational relaxation times for these ions but not with the line width of the absorption spectra. The solute−solvent interactions can be classified into repulsive and attractive parts.[42] The total gas-to-solution solvent shift is a sum of the contributions from the two sources. The frequency shift due to the repulsive part has a different sign from that due to the attractive part. The higher frequency in solution for OCN^- suggests the relative importance of the repulsive part compared to the attractive part. Therefore, it is plausible that the total shift becomes smaller for SCN^- because of the cancellation of two contributions with similar magnitudes even though the magnitude of the shift for each contribution is greater for SCN^- than that for OCN^-. It is a quite interesting problem to investigate the relation between the observed dynamics and the nature of the solvent−solute interaction, namely how the repulsive and attractive parts of the interaction are related with the fast and slow components. It is sometimes argued that the rapid fluctuation results from repulsion and slowly modulating dynamics is caused by an attractive part.[42,43] This tendency might hold for the present case.

As for the microscopic origin of the solute−solvent interaction, it is notable that the dipole moments of the two ions are quite similar, as shown by ab initio calculation. This indicates that the dipole−dipole interaction may be irrelevant for the vibrational frequency fluctuation. On the other hand, the characters of the normal modes for the antisymmetric stretching are quite different between the two ions. In the case of SCN^- the sulfur atom does not move so much during the vibration due to the larger mass, while the vibrational motion is delocalized over the three atoms in the case of OCN^-. Li et al. focused their attention to the normal mode character to explain the difference of T_1 between the two ions on a qualitative level.[19] The difference of the vibrational motion may also be important for the frequency fluctuation, suggesting that rather short range interaction dominates the coupling strength observed in the present study. However, it is absolutely necessary to perform more theoretical work to answer the question on a quantitative level.

6. Conclusion

We have employed three-pulse photon echo spectroscopy to obtain the correlation functions of the vibrational frequency fluctuations of OCN^- and SCN^- in methanol. Two time scales for the decaying components are found for the correlation functions of OCN^- and SCN^-: 100 fs and 4 ps. On the basis of the simulations, we found that the amplitude of the coupling strength to the solvent for SCN^- is larger than that for OCN^-. These observations are in contrast to the results of the vibrational population relaxation times and reorientation times, suggesting weaker solute−solvent interaction for SCN^-. We discuss the possible origins for this difference on the basis of the vibrational Hamiltonian of an anharmonic oscillator coupled to the bath. Even though there remain a couple of issues to be answered, this study provides important results for understanding the solute−solvent interaction of simple ions in polar solvents responsible for the vibrational population relaxation and vibrational dephasing process.

Acknowledgment. This work was supported by a Grant-In-Aid (10206101, 12304036, 13554019, 13640506, 14100100) from Ministry of Education, Science, Sports, and Culture, and a JSPS research grant for the Future Program. Financial supports from the Sumitomo Foundation, the Shimadzu Science Foundation, and the Kurata Foundation are also acknowledged. K. O. is supported by the fellowship from the Japan Society of the

Promotion for Science for Young Scientists. We thank Prof. Yasuhisa Mizutani for valuable discussion and Dr. Mino Yang for providing a source code for the echo calculation.

References and Notes

(1) Oxtoby, D. W. *Annu. Rev. Phys. Chem.* **1981**, *32*, 77.
(2) Fayer, M. D. *Annu. Rev. Phys. Chem.* **2001**, *52*, 315.
(3) Merchant, K. A.; Xu, Q.-H.; Thompson, D. E.; Fayer, M. D. *J. Phys. Chem. A* **2002**, *106*, 8839.
(4) Zanni, M. T.; Hochstrasser, R. M. *Curr. Opin. Struct. Biol.* **2001**, *11*, 516.
(5) Ge, N. H.; Hochstrasser, R. M. *Phys. Chem. Commun.* **2002**, *3*, 1.
(6) Woutersen, S.; Hamm, P. *J. Phys. Condens. Matter* **2002**, *14*, R1035.
(7) Golonzka, O.; Khalil, M.; Demirdoven, N.; Tokmakoff, A. *J. Chem. Phys.* **2001**, *115*, 10814.
(8) Laenen, R.; Simeonidis, K.; Laubereau, A. *Bull. Chem. Soc. Jpn.* **2002**, *75*, 925.
(9) Kropman, M. F.; Bakker, H. J. *Science* **2001**, *291*, 2118.
(10) Madsen, D.; Stenger, J.; Dreyer, J.; Hamm, P.; Nibbering, E. T. J.; Elsaesser, T. *Bull. Chem. Soc. Jpn.* **2002**, *75*, 909.
(11) Fleming, G. R.; Cho, M. *Annu. Rev. Phys. Chem.* **1996**, *47*, 109.
(12) de Boeij, W. P.; Pshenichnikov, M. S.; Wiersma, D. A. *J. Phys. Chem.* **1996**, *100*, 11806.
(13) Joo, T.; Jia, Y.; Yu, J.-Y.; Lang, M. J.; Fleming, G. R. *J. Chem. Phys.* **1996**, *104*, 6089.
(14) Hamm, P.; Lim, M.; Hochstrasser, R. M. *Phys. Rev. Lett.* **1998**, *81*, 5326.
(15) Lim, M.; Hamm, P.; Hochstrasser, R. M. *Proc. Natl. Acad. Sci. U.S.A.* **1998**, *95*, 15315.
(16) Schettino, V.; Hisatsune, I. C. *J. Chem. Phys.* **1970**, *52*, 9.
(17) Jones, L. H. *J. Chem. Phys.* **1956**, *25*, 1069.
(18) Owrutsky, J. C.; Kim, Y. R.; Li, M.; Sarisky, M.; Hochstrasser, R. M. *Chem. Phys. Lett.* **1991**, *184*, 368.
(19) Li, M.; Owrutsky, J. C.; Sarisky, M.; Culver, J. P.; Yodh, A.; Hochstrasser, R. M. *J. Chem. Phys.* **1993**, *98*, 5499.
(20) Owrutsky, J. C.; Raftery, D.; Hochstrasser, R. M. *Annu. Rev. Phys. Chem.* **1994**, *45*, 519.
(21) Ohta, K.; Maekawa, H.; Tominaga, K. Manuscript in preparation.
(22) Maekawa, H.; Tominaga, K.; Podenas, D. *Jpn. J. Appl. Phys.* **2002**, *41*, L329.
(23) Mukamel, S. *Principles of Nonlinear Optical Spectroscopy*; Oxford University: New York, 1995.
(24) Hamm, P.; Hochstrasser, R. M. In *Ultrafast Infrared, Raman Spectroscopy*; Fayer, M. D., Ed.; Marcel Dekker: New York, 2000.
(25) Fourkas, J. T.; Kawashima, H.; Nelson, K. A. *J. Chem. Phys.* **1995**, *103*, 4393.
(26) Tokmakoff, A. *J. Chem. Phys.* **1996**, *105*, 1.
(27) Ohta, K.; Maekawa, H.; Tominaga, K. Unpublished result.
(28) Hamm, P.; Lim, M.; Asplund, M. C.; Hochstrasser, R. M. *Chem. Phys. Lett.* **1999**, *301*, 167.
(29) Asplund, M. C.; Lim, M.; Hochstrasser, R. M. *Chem. Phys. Lett.* **2000**, *323*, 269.
(30) Frisch, M. J.; Trucks, G. W.; Schlegel, H. B.; Scuseria, G. E.; Robb, M. A.; Cheeseman, J. R.; Zakrzewski, V. G.; Montgomery, J. A., Jr.; Stratmann, R. E.; Burant, J. C.; Dapprich, S.; Millam, J. M.; Daniels, A. D.; Kudin, K. N.; Strain, M. C.; Farkas, O.; Tomasi, J.; Barone, V.; Cossi, M.; Cammi, R.; Mennucci, B.; Pomelli, C.; Adamo, C.; Clifford, S.; Ochterski, J.; Petersson, G. A.; Ayala, P. Y.; Cui, Q.; Morokuma, K.; Malick, D. K.; Rabuck, A. D.; Raghavachari, K.; Foresman, J. B.; Cioslowski, J.; Ortiz, J. V.; Stefanov, B. B.; Liu, G.; Liashenko, A.; Piskorz, P.; Komaromi, I.; Gomperts, R.; Martin, R. L.; Fox, D. J.; Keith, T.; Al-Laham, M. A.; Peng, C. Y.; Nanayakkara, A.; Gonzalez, C.; Challacombe, M.; Gill, P. M. W.; Johnson, B. G.; Chen, W.; Wong, M. W.; Andres, J. L.; Head-Gordon, M.; Replogle, E. S.; Pople, J. A. *Gaussian 98*; Gaussian, Inc.: Pittsburgh, PA, 1998.
(31) Krishnan, R.; Binkley, J. S.; Seeger, R.; Pople, J. A. *J. Chem. Phys.* **1980**, *72*, 650.
(32) Dunning, T. H., Jr. *J. Chem. Phys.* **1989**, *90*, 1007.
(33) Woon, D. E.; Dunning, T. H., Jr. *J. Chem. Phys.* **1993**, *98*, 1358.
(34) Szabo, A.; Ostlund, N. S. Modern *Quantum Chemistry: Introduction to Advanced Electronic Structure Theory*; McGraw-Hill: New York, 1989.
(35) Ferrario, M.; Klein, M. L.; MacDonald, I. R. *Chem. Phys. Lett.* **1993**, *213*, 537.
(36) Ferrario, M.; McDonald, I. R.; Symons, M. C. R. *Mol. Phys.* **1992**, *77*, 617.
(37) Oxtoby, D. W. *Adv. Chem. Phys.* **1979**, *40*, 1.
(38) Oxtoby, D. W. *Adv. Chem. Phys.* **1981**, *47*, 487.
(39) Oxtoby, D. W.; Levesque, D.; Weis, J.-J. *J. Chem. Phys.* **1978**, *68*, 5528.
(40) Morita, A.; Kato, S. *J. Chem. Phys.* **1998**, *109*, 5511.
(41) Rey, R.; Hynes, J. T. *J. Chem. Phys.* **1998**, *108*, 142.
(42) Myers, A. B.; Markel, F. *Chem. Phys.* **1990**, *149*, 21.
(43) Schweizer, K. S.; Chandler, D. *J. Chem. Phys.* **1982**, *76*, 2296.